# Axial Compression and Buckling Behaviors of Hollow Square Glued Bamboo Scrimber Column: An Experimental Study

Xian Yu,<sup>a,\*</sup> Gang Yao,<sup>a</sup> Yang Yang,<sup>a</sup> Jianming Zhou,<sup>b</sup> and Lin Guo <sup>a</sup>

Hollow glued bamboo scrimber (HGBS) columns constructed from bamboo scrimber plates were proposed as structural load-bearing components instead of traditional solid bamboo columns to enhance the stable load of columns without increasing material consumption. To analyze the mechanical behavior of HGBS columns, tests were first conducted on the elastic modulus and compressive strength of bamboo scrimber made from Neosinocalamus affinis to theoretically assess the material's mechanical properties. A total number of 22 HGBS square cross-section with dimensions of 100 mm columns, varying slenderness ratios and hollow ratios, were fabricated with glued and nailed connections. These columns were subjected to axial compression tests to evaluate their failure modes, axial stiffness, bearing capacity, and ductility. Theoretical calculation models were developed for the HGBS columns to estimate load-bearing capacity. This research provides a comprehensive understanding of HGBS columns and broadens their potential applications in structural engineering.

DOI: 10.15376/biores.20.4.9678-9698

Keywords: Bamboo structure; Hollow glued bamboo scrimber (HGBS); Axial compressive behavior; Load-bearing capacity; Theoretical calculation model

Contact information: a: School of Civil Engineering, Chongqing University, No.174 Shazheng Road, Chongqing, 400044, China; b: Sichuan Zhuyuan Technology Co., Ltd., No. 30, Shengke Road Section 2, Hongya Economic Development Zone, 620300, China;

# INTRODUCTION

Bamboo, with its renewable nature, rapid growth rate, and carbon sequestration ability, stands out as a lightweight material that is inherently resistant to seismic activity. This aligns well with the principles of sustainable development (De Flander et al. 2009; Meng et al. 2023; Zhang et al. 2024;). Despite its advantages, the direct use of bamboo in structural engineering presents challenges, primarily due to its small diameter and relatively soft texture (Mahdavi et al. 2011; Li et al. 2013; Fei et al. 2019). The innovation of bamboo scrimber, through strategic reorganization, enhances its strength and ductility while maintaining mechanical stability. This positions bamboo scrimber as a viable option for structural applications with considerable potential (Qi et al. 2015; Li et al. 2016; Kumar et al. 2016; Sharma and van der Vegte 2020; Dauletbek et al. 2023). The strength-to-weight ratio of bamboo scrimber composite surpasses that of Q235 steel by four or five times, and its tensile and compressive strength are twice those of the esteemed purple sandalwood. However, the modulus of elasticity is not correspondingly increased relative to the source material, which could result in big deformations under external loads before reaching strength failure. With the same amount of material, the moment of inertia of a hollow column's cross-section is greater than a solid column's cross-section, resulting in the hollow column having a higher stable load-bearing capacity than the solid column (Wang 2020). Therefore, it is

<sup>\*</sup>Corresponding author: yuxian@stu.cqu.edu.cn

worthwhile to further explore the concept of using hollow cross-sectional designs for primary load-bearing columns to enhance rigidity and material efficiency.

Relevant investigations have been extensively conducted to explore the mechanical properties and engineering applications of engineered bamboo materials (Li et al. 2015, 2019; Kurt and Tomak 2019; Sharma and van der Vegte 2020). Meanwhile, there have also been many studies focusing on beams (Wei et al. 2017; Zhong et al. 2017; Yang et al. 2020), wall panels (Xiao et al. 2015; Wang et al. 2017), and joints (Jensen and Quenneville 2011; Leng et al. 2021). Recent research on bamboo scrimber columns mainly has focused on the axial compression performance or buckling behavior of solid material. Ke et al. (2014) experimentally investigated the mechanical properties of recombined bamboo columns used in frame structures and analyzed the influence of different slenderness ratios on the load-bearing capacity. Su et al. (2015) experimentally studied the axial compression performance of Bamboo Parallel Strand Lumber (PBSL) columns and found that the compression performance of PBSL columns was superior to that of other types of recombined bamboo columns. Li et al. (2015) investigated the axial compression performance of recombined bamboo columns with different slenderness ratios and found that the stress-strain curves exhibited nonlinearity. They proposed a material constitutive relationship based on the Ramberg-Osgood model to accurately describe the nonlinear mechanical behavior of recombined bamboo. The buckling performance of bamboo scrimber columns is one of the research hotspots. Wei et al. (2025) experimentally investigated the axial compression behavior of a new type of laminated bamboo tube and developed a new predictive model to assess the buckling behavior of bamboo tubes under axial compression. Tan et al. (2021) experimentally and numerically investigated the buckling behavior of recombined bamboo columns under axial compression and found that initial geometric imperfections and material nonlinearity affected the buckling performance. They proposed a nonlinear buckling analysis method considering initial imperfections. Hollow components have a higher moment of inertia under the same cross-sectional area, which can enhance the bearing capacity of the components to a certain extent and improve the material utilization rate

Regarding the mechanical behavior of bamboo-based hollow columns, Dewi et al. (2018) revealed three typical failure modes of medium and long columns through systematic tests on 30 specimens – material fragmentation, inelastic buckling, and wall cracking. Based on this, Su et al. (2024) innovatively proposed an anisotropic plate model with a width correction coefficient to better predict the critical buckling load of hollow columns. Further, Zhou et al. (2023) constructed box columns using hot-pressed bamboo fiber-reinforced plates and quantified the influence law of high-to-low width ratio on the overall buckling mode through the combination of experiments and finite element methods. Although there have been numerous experimental studies on the mechanical properties of bamboo scrimber columns, there are still some deficiencies. Particularly, the research on bamboo scrimber hollow columns is extremely limited at present. Only a few studies have explored the failure modes of hollow-section bamboo composite columns, lacking systematic analysis of key parameters such as crosssectional shape, plate thickness, and hollow rate, and failing to form a unified design theoretical framework. The existing bearing capacity equations are mostly based on the test data of specific cross-sectional forms and have not established a universal buckling design theoretical framework. These research gaps severely restrict the optimization design and application promotion of bamboo scrimber hollow columns in engineering practice.

This study explored the bearing capacity and stability of hollow glued bamboo scrimber (HGBS) columns and investigated their failure modes. Changes in mechanical

properties of HGBS columns were also analyzed with comparation of solid columns. This study also examined the impact of different slenderness and hollow ratios on load-bearing capacity, conducted a comparative analysis of existing standards, and developed a calculation equation. The ultimate goal is to create a robust analytical model for their axial compression capacity, promoting the sustainable use of bamboo in construction.

#### **EXPERIMENTAL**

#### **Materials**

The column elements utilized in this experiment were sourced from Hongya County, Meishan City, Sichuan Province, and constructed from Neosinocalamus bamboo, as shown in Fig. 1. The species of bamboo, age, distribution of internodes, fiber orientation, uniformity of resin impregnation, and thermal pressing parameters are all factors that affect the variation of raw material properties.

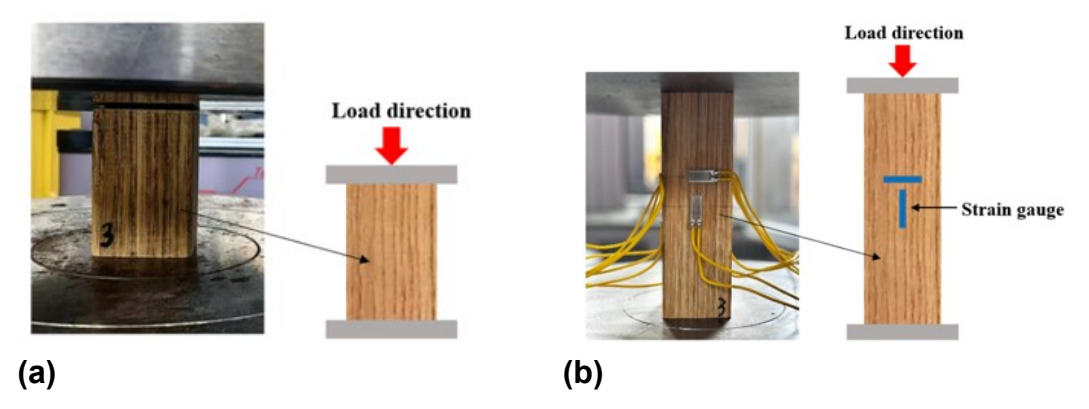
To ensure the consistency of test performance, the raw materials used for this test were from the same batch of raw bamboo materials, and the bamboo scrimber plates were produced in the same way. Five samples of the plates from this production batch were selected to test the density, moisture content, and material properties. The coefficient of variation is controlled within 10% to avoid inherent variability. For materials that had not undergone tests yet, they were protected by covering with plastic films and placing desiccants.



Fig. 1. Bamboo scrimber production process

Physical properties of materials

The compressive strength of bamboo scrimber in the longitudinal direction was determined according to the specifications outlined in LY/T 3194 (2020).



**Fig. 2.** Schematic diagram of material mechanical performance test loading. (a) Compressive test (b), Compressive modulus test

The specimens had a rectangular cross-section measuring  $20 \text{ mm} \times 20 \text{ mm}$  and the length of 30 mm along the longitudinal axis. To measure the compressive elastic modulus in the same direction, the guidelines provided in GB/T 15777 (2017) were followed. These specimens also featured a rectangular cross-section of  $20 \text{ mm} \times 20 \text{ mm}$  with the length of 60 mm. Figure 2 presents the configuration of the loading setup, while Table 1 outlines the detailed steps for testing the mechanical performance of the materials.

Table 1. Test Results of Material Performance

Performance	Mean	Characteristic	Standard	Coefficient of
Parameters	Value	Value	Deviation	Variation
Compressive strength along the grain	90.3	81.6	5.28	5.85
	(MPa)	(MPa)	(MPa)	(%)
Compressive modulus along the grain	33.8	27.4	3.93	11.6
	(GPa)	(GPa)	(GPa)	(%)
Density	11.5	11.1	0.26	2.3
	(kg.m <sup>-3</sup> )	(kg.m <sup>-3</sup> )	(kg.m <sup>-3</sup> )	(%)
Moisture content	2.3	2.26	0.02	0.9
	(%)	(%)	(%)	(%)

#### **Specimen Preparation**

To investigate the bearing capacity of HGBS and their potential to enhance stability, as well as to study the main factors affecting the bearing capacity and their impact levels, this study designed an experimental array consisting of eleven groups, each comprising two specimen. The specific properties of the HGBS columns are detailed in Table 2. For example, HS1200T20 represents the HGBS column with a height of 1200 mm, and has a plate thickness of 20 mm.

Sequence Number	Specimen IDs	Length (mm)	Height*Width (mm²)	Thickness (mm)	Number
1	HS300T20	300	100×100	20	2
2	HS600T20	600			
3	HS900T20	900			
4	HS1200T20	1200			
5	HS1500T20	1500			
6	HS1800T20	1800			
7	HS2400T20	2400			
8	HS1200	1200		solid	
9	HS1200T10	1200		10	
10	HS1200T30	1200		30	
11	HS1200-E	1200	180×180	30	

Table 2. Specific Properties of the HGBS Columns

The fabrication process involved assembling four plates orthogonally aligned into a box-shaped section following grinding and no more than 25 °C drying to ensure a moisture content below 11%. Polyurethane glue was uniformly applied to all joining surfaces. The assembly was then subjected to compression perpendicular to the axis, but clamping, and left to cure naturally for 8 hours. Self-tapping screws of 4.2 mm diameter and 32 mm length were affixed using a nail gun, with the nail holes sealed using a glue and sawdust mixture. The columns were finally trimmed and finished to produce the ready-to-test hollow column specimens, as shown in Fig. 3.

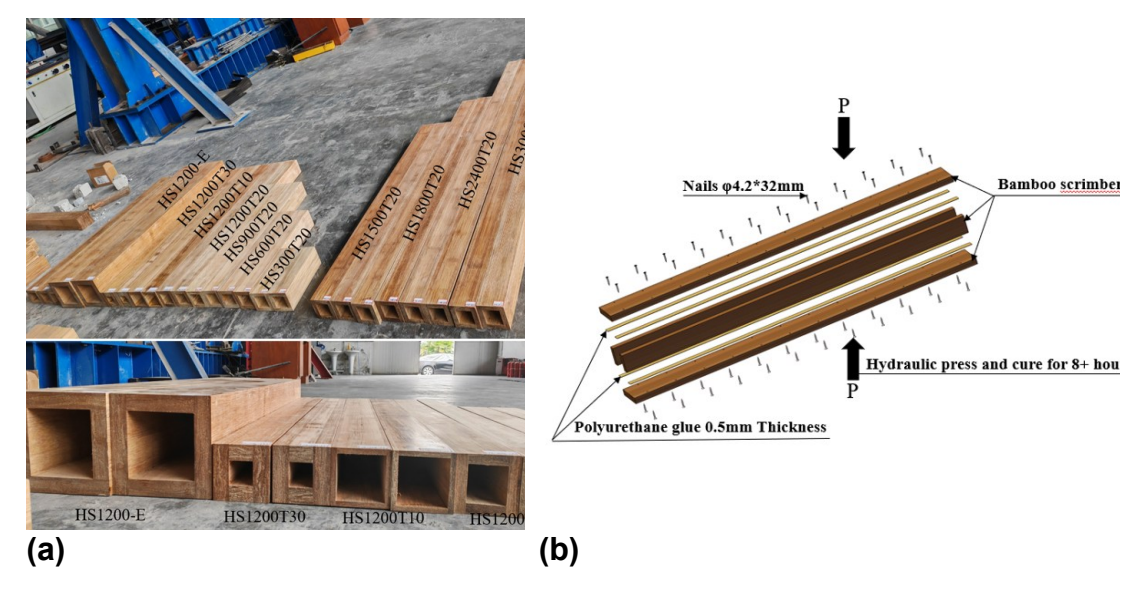


Fig. 3. Manufacturing of HGBS columns. (a) Finished product, (b) Production process

#### **Experiment Setup**

The compression tests of the HGBS columns were carried out at the Civil Engineering Structures Laboratory, Jiang'an Campus, Sichuan University. A microcomputer-controlled servo-hydraulic pressure testing machine was employed for the test, shown in Fig. 4.

<sup>\*</sup> HS=Hollow Section, T=Thickness, E=Expanded Section to 180×180 mm<sup>2</sup>

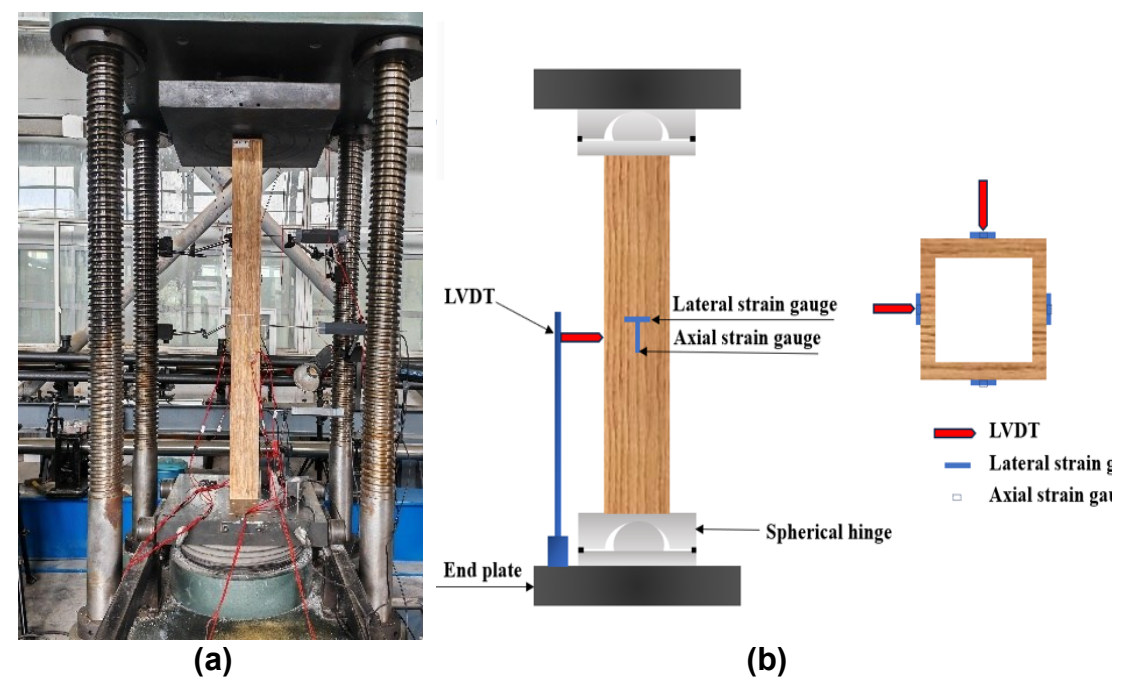


Fig. 4. Diagram of the loading device. (a) Test site equipment, (b) Diagram of the device

The maximum load capacity of this equipment was 20,000 kN, and its displacement control system achieved a resolution of 0.01 mm through closed-loop feedback. According to GBT50329 (2012), the columns were supported by ball joints at both ends, providing rotation freedom about two orthogonal axes while restricting lateral translation via hardened steel guide plates. Prior to loading, a two-step alignment protocol was implemented: (1) laser alignment of the specimen's longitudinal axis with the actuator centerline, (2) pre-loading to 100 kN to verify strain symmetry. Strain gauges (120-50AA), with temperature compensation using dummy gauges, were attached vertically and horizontally at the midspan of all four sides of each column, while a YWD-100 displacement sensor with arrange of 0 to 100 mm, was placed at the midspan to measure lateral displacement. Systematic errors from machine compliance were mitigated by conducting three zero-load pre-loadings. All strain and displacement data were collected in real time using the TDS-530 signal acquisition instrument.

#### **RESULTS AND DISCUSSION**

# Failure Modes Controlled by Slenderness Ratio

For the groups with different slenderness, the experimental analysis identified three primary failure modes in HGBS, including strength failure, combined strength and instability failure, and instability failure alone. Strength failure was predominantly marked by bamboo splitting and the delamination of adhesive layers, with clear signs of cracking where primary and secondary bonding occurred, including instances where nails were pulled apart. Notably, strength failures were observed at column lengths of 300 mm and 600 mm. Initial fractures were first noted at the secondary bonding sites (e.g., HS300T20-1), with subsequent bamboo yielding at both column ends and the center, followed by further cracking at primary bonding sites. In HS600T20-1, splitting commenced at 5 cm from the base, quickly followed by cracking at the glued joint. The HS600T20-2 specimen initially bent 10 cm below the midpoint, leading to subsequent cracks at both bonding interfaces and eventual nail separation. When the length of HGBS column was less than or equal to 600 mm, the final form of destruction was

manifested as crashing, splitting, delamination, and end bearing failure, as shown in Fig. 5. (1). For columns measuring 900 mm and 1200 mm, both strength and instability failures were observed. The HS900T20-1 column displayed S-shaped bending, as shown in Fig. 5. (e). This is due to material yielding, progressing to cracks at both the secondary and primary adhesive joints. Similarly, the HS1200T20-1 column demonstrated subtle S-shaped deformations, starting with cracking at the upper left secondary bonding area and quickly propagating to the right, leading to delamination and nail separation, forming an S+C configuration, as shown in Fig. 5. (f). Columns with lengths of 1500 mm, 1800 mm, and 2400 mm exclusively exhibited instability failures. For instance, HS1500T20-1 and HS1500T20-2 showed C-shaped bending towards alternating axes, as shown in Fig. 5. (g). HS2400T20-2 experienced premature material failure due to initial defects, with no bending observed.

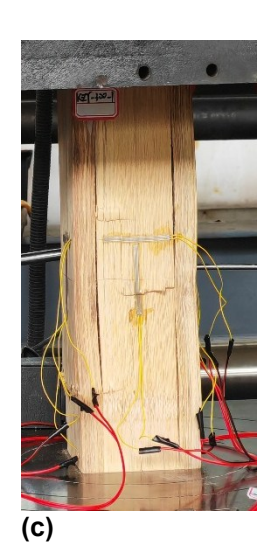
The critical buckling load decreased as the slenderness ratio increased, leading to a higher likelihood of instability failures, which are consistent with the predictions of Euler's buckling theory (Eq. 1),

$$P_{cr} = \frac{\pi^2 EI}{I^2} \tag{1}$$

where  $P_{cr}$  is Euler critical buckling load, E is the modulus of elasticity, and I is the length of the column. However, the presence of localized material failures suggests that the behavior of HGBS columns is also influenced by the anisotropic nature of the bamboo scrimber material, which is not fully captured by Euler's buckling theory. Furthermore, the failure modes of HGBS columns differ from those of solid bamboo columns under similar loading conditions (Goonewardena  $et\ al.\ 2024$ ). Solid bamboo columns typically exhibit more uniform bending and less localized cracking due to their homogeneous structure. In contrast, the hollow design of HGBS columns introduces stress concentrations at the adhesive joints and layer plates, leading to complex failure patterns such as S+C configurations. This highlights the need for specialized mechanical models to predict the behavior of hollow bamboo structures.









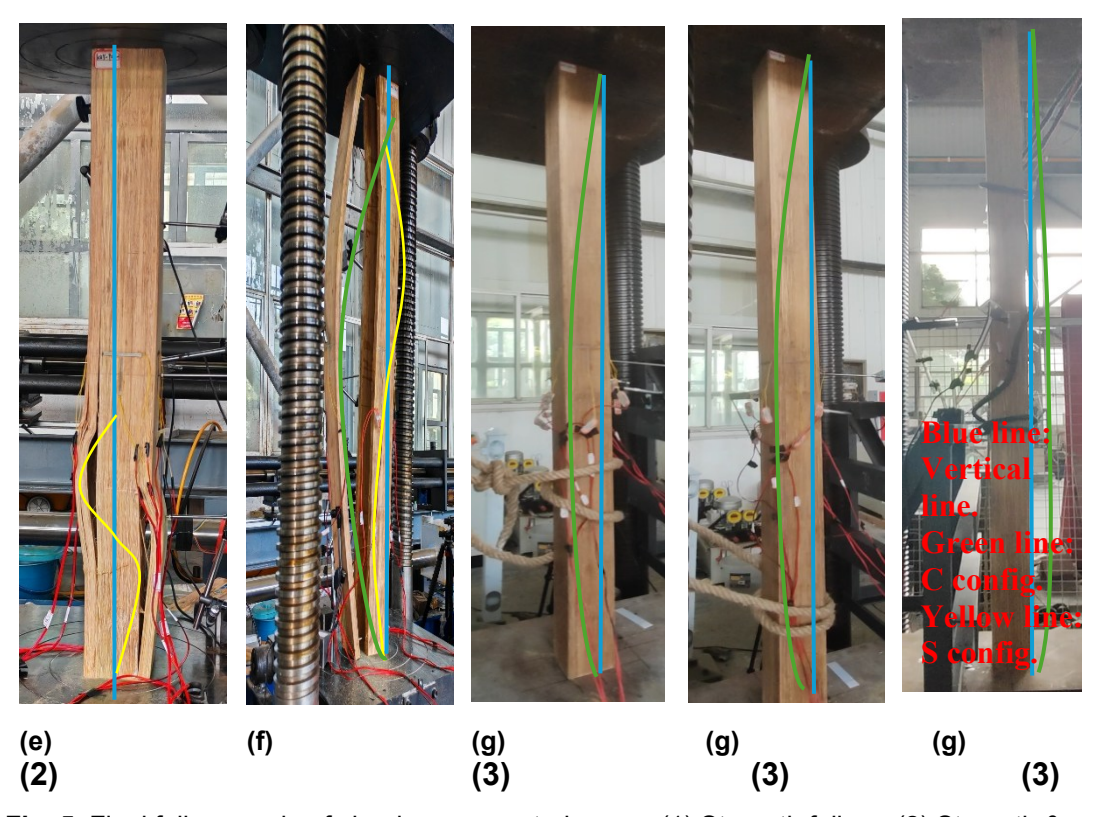


**Fig. 5.** Final failure mode of slenderness control group. (1) Strength failure, (2) Strength & Instability failure, (3) Instability failure; (a) Crushing, (b) Splitting, (c) Delamination, (d) End bearing failure, (e) S shape+Delamination, (f) S+C shape+Nails pulling out, (g) C shape

#### **Failure Modes Controlled by Hollow Ratio**

For the groups with different hollow ratio, the failure mode exhibited simultaneous occurrences of material failure and structural instability, as shown in Fig. 6. HS1200-10-1 underwent significant lateral deformation, leading to the collapse of the layer plate and the cracking of the adhesive layer at the lower end. HS1200-10-2 exhibited a sudden rupture in the lower half of the layer plate following lateral deformation. One of the plates in HS1200-20-1 showed obvious bending deformation and the nails had been pulled apart. Meanwhile, HS1200-20-2 only showed overall bending deformation. This might be related to the assembly process of the HGBS columns. For HS1200-30-1, the cracking in the adhesive layer occurred after lateral deformation. For the solid engineered bamboo group, the interlayer of layer plate cracked after lateral deformation. HS1200-E showed minimal lateral deformation, but it still experienced cracking in the adhesive layer. The study highlights the stochastic nature of failure in hollow bamboo columns, which can be attributed to variations in material consistency and adhesive bonding during production. Columns of 300 and 600 mm heights primarily suffered from material failures such as bamboo splitting and adhesive delamination. In contrast, columns of 900 and 1200 mm heights showed a blend of strength and instability failures, characterized by material degradation and buckling. Columns taller than 1500 mm consistently exhibited unstable fractures, primarily manifesting as C-shaped bending along random axes. The study also noted that buckling typically presented as minor lateral deflections resulting from initial bending and eccentric loading during testing. Increasing slenderness ratios exacerbated these effects, notably affecting load-bearing capacity and leading to a sharp increase in deflection upon reaching the critical load value. The hollow ratio also affects the damage pattern, in the case of using the same material, increasing the hollow ratio can improve the lateral stiffness and reduce lateral displacement.

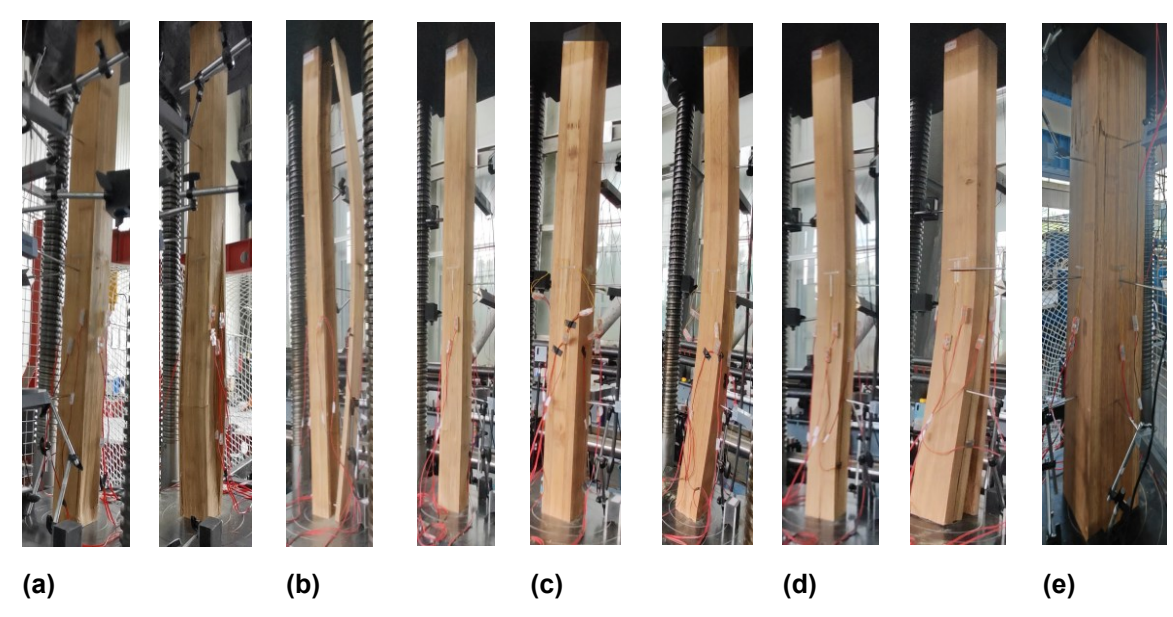


**Fig. 6.** Final failure mode-hollow ratio control group. (a) HS1200-T10, (b) HS1200-T20, (c) HS1200-T30, (d) HS1200, (e) HS1200-T

#### **Axial Load-displacement Behavior**

When fixing the hollow ratio, columns with the length less or equal to 1200 mm showed minimal variation in load-bearing capacity, as shown in Fig. 7. (a). This suggests that the influence of the slenderness ratio is limited, and the material's inherent strength governs the structural response. As the length of the column was increased, the stiffness of column decreased, and the carrying capacity began to decline, as shown in Fig. 7. (b). This indicates a transition from material-driven failure modes to stabilitydriven behavior. Buckling effects became more prominent these columns. The effect of hollow ratio is shown in Fig. 7. (c) and (d). Increasing hollow ratio led to both reduced stiffness and lower load-bearing capacity. For instance, the load-bearing capacity of the solid column was four times that of the hollow column with a plate thickness of 10 mm, and its axial compression ratio was also three times that of the latter. By comparing the hollow columns of HS1200-E and solid columns with similar material usage, it can be seen that the hollow columns performed excellently in terms of bearing capacity, while their ductility was half that of the solid group. This indicates that the hollow section tends to concentrate stresses, accelerating the onset of local failures and reducing the column's stiffness.

The experimental results are shown in Table 3. The initial stiffness, denoted as K, is determined based on the load values at the elastic stage  $F_0$  and  $F_1$ . This calculation considers two load values: 100 and 200 kN. The axial displacement values corresponding to these loads are represented by  $\Delta_0$  and  $\Delta_1$  respectively. And the calculation of initial stiffness is shown in Eq. 2.

$$K = \frac{F_1 - F_0}{\Delta_1 - \Delta_0} \tag{2}$$

The ductility coefficient was calculated using Eq. 3,

$$\mu = \frac{u_m}{u_y} \tag{3}$$

where  $u_{\rm m}$  is the ultimate displacement of the component, and  $u_{\rm y}$  is the yield displacement of the component. Because the specimen behaves as a non-ideal elastoplastic body, the yield point is calculated using the energy equivalence method (Feng *et al.* 2017).

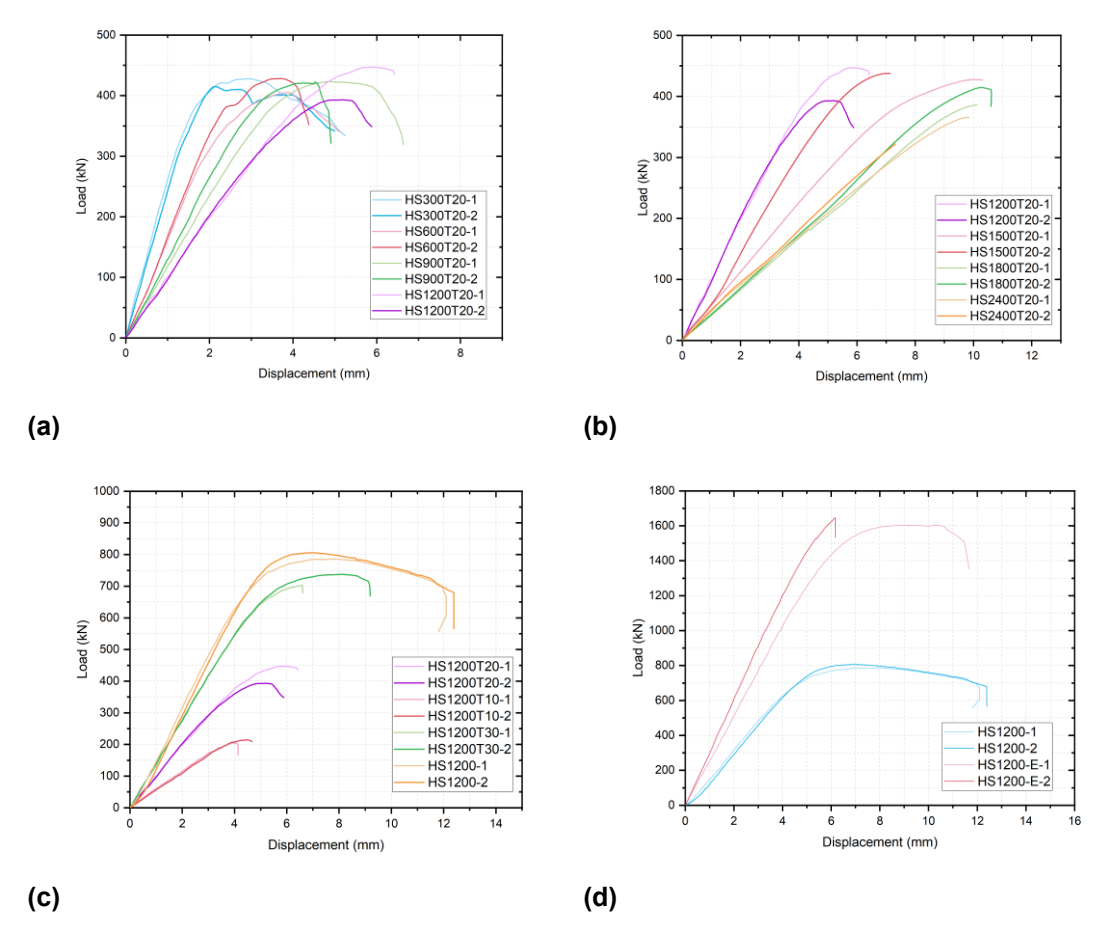


**Fig. 7.** Load-axial displacement diagram. (a) the slenderness group 300mm-1200mm, (b) the slenderness group 1200mm-2400mm, (c) the hollow ratio group, (4) the hollow ratio group

From the evolution pattern of the ductility coefficient index, it can be seen that under the condition that the hollow ratio remained unchanged, the ductility of the HGBS column exhibited a nonlinear change behavior. Specifically, as the slenderness ratio was increased, the ductility coefficient showed a trend of first decreasing and then increasing. The test data showed that when  $\lambda \leq 44.6$ , the ductility coefficient continuously decreased from the initial 1.14 to 0.09, with a reduction of 92%; while when  $\lambda \geq 53.5$ , the ductility coefficient rose from 0.24 to 0.53, with an increase of over 100%. This nonlinear response reveals that there is a critical correlation between the ductility index of the HGBS column and the slenderness ratio. The critical slenderness ratio was observed in the approximate column length range of 1500 to 1800 mm

# \_bioresources.cnr.ncsu.edu

 Table 3. Experiment Results of HGBS Columns

Specimen	Solid	Hollow	Material		Peak Load (kN)				Elastic Modulus (GPa)						Ductility	
IDs	Area (mm²)	Ratio (%)	Efficiency (kN/mm²)	.*	S1	S2	Ave.	SD	COV	S1	S2	Ave.	SD	COV	Stiffness	Coefficient
HS300T20	6400	36	6.6%	8.9	427.8	415.1	421.5	6.3	1.5	39.9	38.0	38.9	0.9	2.3	249.11	1.14
HS600T20			6.7%	17.8	405.4	428.1	416.7	11.3	2.7	26.9	29.0	27.9	1.1	3.9	178.86	0.49
HS900T20			6.6%	26.7	423.1	420.6	421.9	1.3	0.3	18.5	20.9	19.7	1.2	6.1	126.14	0.32
HS1200T20			6.5%	35.6	420.1	393.0	406.0	13.6	6.5	15.8	16.8	16.3	0.5	3.1	104.48	0.27
HS1500T20			6.7%	44.6	427.1	1	427.1	/	/	12.5	13.2	12.9	0.3	2.3	82.41	0.09
HS1800T20			6.3%	53.5	386.2	414.7	400.5	14.2	3.5	9.4	9.7	9.5	0.1	1.1	61.11	0.24
HS2400T20			4.8%	64.9	358.6	256.2	307.4	51.2	16.6	8.7	9.1	8.9	0.1	1.1	57.04	0.53
HS1200	10000	0	8.0%	41.6	785.4	805.7	795.6	10.1	1.3	16.9	17.3	17.1	0.1	5.8	170.97	1.26
HS1200T10	3600	64	5.8%	32.5	204.9	214.3	209.6	4.7	2.2	14.8	14.1	14.5	0.3	2.1	52.10	0.25
HS1200T30	8400	16	8.6%	38.6	702.6	737.3	719.9	17.3	2.4	17.7	18.4	18.0	0.4	2.2	151.46	0.75
HS1200-E	18000	44	9.1%	19.2	1602.7	1646.4	1646.4	21.8	1.3	14.9	17.3	16.1	1.2	7.5	289.39	2.76

From the mechanical mechanism analysis, this change trend can be attributed to the transformation of the structural failure mode. In the low slenderness ratio range, the component is mainly controlled by the material strength for crushing failure, the fiber reinforcement effect of the component is fully exerted, resulting in a higher ductility reserve. However, as the slenderness ratio increases, the component gradually enters the failure mode dominated by elastic instability, and the lateral deflection caused by the second-order effect intensifies the strain concentration of the fibers at the edge of the section, leading to a decrease in ductility. When exceeding the critical slenderness ratio, the failure mode of the component changes to ductile buckling that can maintain a large deformation after instability.

#### **Load-strain Behavior**

The load-strain curves in Fig. 8 show that the longitudinal elastic modulus of HGBS was lower than its transverse elastic modulus. This disparity is due to the anisotropic nature of bamboo fiber orientation, where fibers are more aligned along the longitudinal direction, leading to a better response under longitudinal loading compared to the transverse direction, where the structure is less fiber-dominant and hence stiffer. The elastic-plastic behavior transition occurs at the inflection point of the curve (where the slope approaches zero), typically near the peak load. Beyond this critical strain, nonlinear deformation becomes dominant. During experiments, a distinct sound of brittle fracture of bamboo fibers was heard, which was accompanied by fiber delamination and laminate cracking. These phenomena are directly associated with the structural collapse phase.

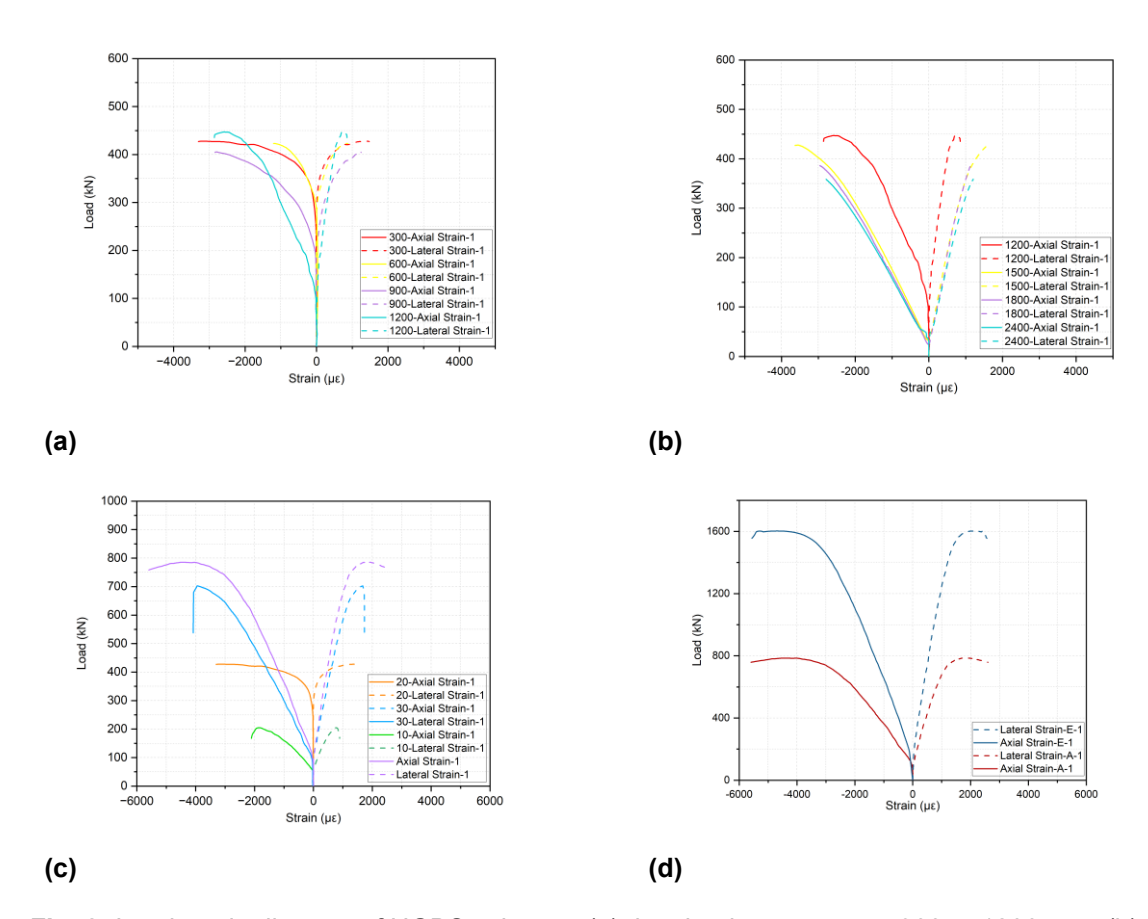


**Fig. 8.** Load-strain diagram of HGBS columns. (a) the slenderness group 300 to 1200 mm, (b) the slenderness group 1200 to 2400 mm, (c) the hollow ratio group, (d) the hollow ratio group

For columns with a length of 1200 mm or less, a distinct plastic stage was maintained after the inflection point, as shown in Fig. 8. (a), whereas columns longer than 1200 mm exhibited a much shorter plateau period, as shown in Fig. 8. (b). Thus, columns with higher slenderness ratios possess lower stiffness, are more susceptible to instability-induced failure, and reach their bearing capacity limit before the full performance is utilized. This conclusion aligns with experimental observations, where columns with larger slenderness ratios are less likely to exhibit visible material failure phenomena prior to structural collapse. In the case of varying hollow ratios, both the ultimate longitudinal load and transverse ultimate load decrease as the hollow ratio increases, as shown in Fig. 8(c) and (d). This trend is expected, as increasing the hollow ratio reduces the cross-sectional area available to resist both longitudinal and transverse loads. The higher hollow ratio weakens the structural integrity of the column by concentrating stress around the periphery, thereby lowering the ultimate load capacity in both directions.

In the low slenderness ratio range, the component was mainly controlled by the material strength for crushing failure, and at this time, the fiber reinforcement effect of the component was fully exerted, resulting in a higher ductility reserve. However, as the slenderness ratio increased, the component gradually entered the failure mode dominated by elastic instability, and the lateral deflection caused by the second-order effect intensified the strain concentration of the fibers at the edge of the section, leading to a decrease in ductility. When exceeding the critical slenderness ratio, the failure mode of the component changed to ductile buckling that can maintain a large deformation after instability. This rule can still be found in the control group of hollow ratio. When  $\lambda = 32.5$ , the ductility coefficient of HS1200-10 was 0.25, and it increased to 1.26 of HS1200 ( $\lambda = 41.6$ ). However, for the group of HS1200-E ( $\lambda = 19.2$ ), the ductility coefficient increased to 2.76. This indicates that the hollow ratio also affects the slenderness ratio to some extent, thereby influencing the ductility of the component.

# **Discussions on Bulking Coefficient**

The experimental results were compared with standards NDS (2005), Eurocode 5 (2001), and GB 50005 (2003). The relevant calculation formula for axial compressive bearing capacity is listed in Table 4. Figure 9 shows a comparison of the prediction of the bulking coefficient of the norms with the experimental results as a function of  $\lambda$ . As observed, from the perspective of the comparison group regarding the slenderness ratio, for columns wit  $\lambda \le 44.6$ , all the norms overestimated their stability coefficients. Based on the failure modes of the tests, it is possible that the local buckling was caused by the crushing and delamination that occurred during the compression process of the HGBS columns. For columns with  $\lambda > 44.6$ , the test results were more in line with the curves of various norms, especially for EU5, but there were still certain errors. This might be due to local instability of the plates or the construction process. From the perspective of the hollow ratio control group, for the HGBS columns with a hollow ratio less than 36%, all the specifications were able to well estimate their strength. However, more data are still needed to support it. For the cases where the hollow ratio was greater than or equal to 36%, there were evident deviations between the various specifications, and this situation might be related to the connection method between the HGBS layers. However, these specifications default to the applicable objects of solid cross-section components. According to the results derived from the existing wood structure specifications, their accuracy is insufficient, especially when the slenderness ratio is within 44.6.

 Table 4. Comparison of Formulas under Different Norms.

Chinese GB50005-2017	Eurocode 5	NDS					
$F = \varphi A f_c$	$F = \varphi A f_c$	$F = AF_c$					
$\left[\frac{\alpha_c \pi^2 \beta E_k}{\lambda^2 f_{ck}}  \text{for } \lambda > \lambda_{\text{rc, test}},\right]$	$\varphi = \frac{1}{k + \sqrt{k^2 - \lambda_{rel}^2}}$	$F_{c}^{'} = F_{c}(C_{D})(C_{M})(C_{t})(\varphi)$					
$\varphi = \begin{cases} \frac{\alpha_c \pi^2 \beta E_k}{\lambda^2 f_{ck}} & \text{for } \lambda > \lambda_{\text{rc, test}}, \\ \frac{1}{1 + \frac{\lambda^2 f_{ck}}{b_c \pi^2 \beta E_k}} & \text{for } \lambda \leq \lambda_c. \end{cases}$							
$\lambda_c = c_c \sqrt{rac{eta E_k}{f_{ck}}}$	$k = 0.5[1 + \beta_c(\lambda_{rel} - 0.3) + \lambda_{rel}^2]$	$\varphi = \frac{1 + F_{cE}/F_c^*}{2c} - \sqrt{\left(\frac{1 + F_{cE}/F_c^*}{2c}\right)^2 - \frac{F_{cE}/F_c^*}{c}}$					
		$F_{cE} = \frac{0.822E_{\min}^*}{(K_e l / d)^2}$					
		$E_{\min}^* = E_{\min}(C_m)(C_t)$					
	$\lambda_{rel} = rac{\lambda}{\pi} \sqrt{rac{f_{ck}}{E_k}}$	$E_{\min} = 1.13E[1 - 1.645(COV_E)]/1.66$					
		$F_{\rm c}^* = F_{\rm c}(C_D)(C_M)(C_{\rm t})$					
$A$ is the compression area of the column. $f_c$ is the compressive strength along the grain. $\varphi$ is the buckling coefficient. $\lambda$ is the slenderness of columns. $\lambda_c$ is the critical slenderness ratio. $f_{ck}$ is the characteristic value of the compressive strength along the grain. $E_k$ is the characteristic value of modulus of elasticity. The values of $a_c$ , $b_c$ , $c_c$ and $\beta$ can be taken as 0.91, 3.69, 3.45, and 1.05, respectively.	$A$ is the compression area of the column. $f_c$ is the compressive strength along the grain. $\varphi$ is the buckling coefficient. $\lambda_{rel}$ is the relative slenderness ratios. $\beta_c$ is a factor for column within the straightness limits, refer to glulam take 0.1. $f_{ck}$ is the standard value of compressive strength. $E_k$ is the standard modulus of elasticity.	$F_c'$ is the adjusted design value parallel to grain. $F_c$ is the reference design value parallel to grain. $C_D$ is the load duration factor, taken as 1.0 for short term loading. $C_M$ is the wet service factor and is suggested to adopt 1.0 for current study (moisture content less than 16%). $C_t$ is the temperature factor, taken as 1.0 for current study (environment temperature less than 150 °F). $\varphi$ is the column stability factor. $F_{cE}$ is the critical buckling design value for compression members; $F_c^*$ is the reference compressive design value parallel to grain. $C_t$ is taken as 0.9 refers to glued laminated timber. $C_t$ is the reference modulus of elasticity. $C_t$ is the adjusted modulus of elasticity. $C_t$ is the buckling length coefficient. $C_t$ is the coefficient of variation for modulus of elasticity, taken as 0.1.					

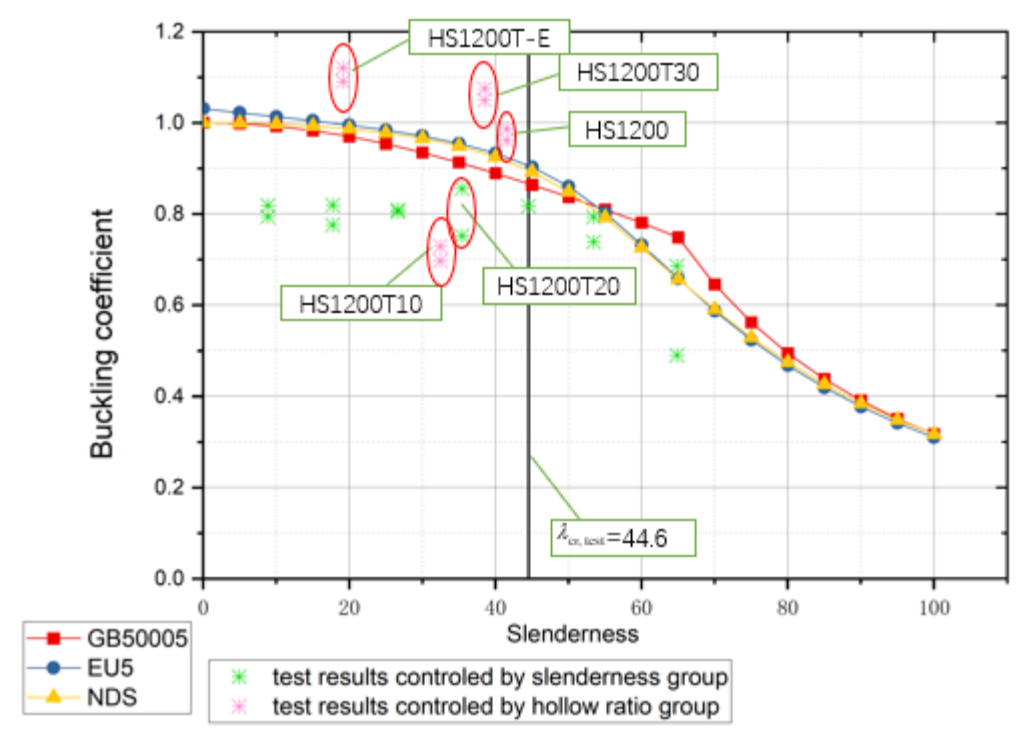


Fig. 9. Buckling coefficient-slenderness for all specimens

None of the specifications consider the local buckling of hollow components and the effectiveness of laminated plate connections. Therefore, it is crucial to develop a prediction model applicable to the full range of long-to-short ratios for HGBS columns. Such equations are essential for ensuring safety.

#### Theoretical Implications

The analysis of axial load-bearing capacity in columns is a fundamental research topic in structural mechanics. For columns composed of typical engineering materials, the axial capacity of slender columns is generally analyzed using Euler's buckling theory, which accurately predicts failure due to buckling. In contrast, the load-bearing capacity of squat columns is largely determined by the material's compressive strength, with crushing being the primary failure mode, as seen in materials like timber.

However, the behavior of hollow short columns cannot be fully characterized by material strength alone. The hollow geometry introduces complexities such as localized stress concentrations, making simple material-based models insufficient. For intermediately slender columns, the failure mode is more intricate, as it involves a combination of buckling instability and material failure, leading to a mix of buckling and material damage that is not easily captured by conventional approaches.

In this paper, the tangent modulus theory is applied to evaluate the axial capacity of HGBS columns. This method allows for a more refined analysis by incorporating the non-linear stress-strain behavior of the material and the geometric effects due to slenderness. The tangent modulus theory adjusts the stiffness of the column as it undergoes inelastic deformations, providing a more accurate representation of the column's load-bearing behavior. This approach is particularly relevant for HGBS columns, as it accounts for the complex interaction between buckling and material degradation, especially in hollow columns, where failure modes are more varied and challenging to predict with simple material strength models. To determine the axial load capacity of HGBS columns,

we apply both Euler's buckling theory and the tangent modulus theory step by step. These two methods are applicable depending on whether the column is slender or subject to inelastic behavior.

# **Euler's Buckling Theory for Slender Columns**

For slender columns, Euler's buckling theory is used to determine the critical load at which buckling occurs. The Euler buckling load is calculated using the Eq. 4,

$$P_{cr,hollow} = \frac{\pi^2 EI(\psi)}{(Kl)^2} \tag{4}$$

where K is the effective length factor, which depends on the boundary conditions. K=1 for columns that are pinned at both ends. E is the elastic modulus of the HGBS material. The critical load may also be modified to account for variations in hollow ratio  $\psi$ , where  $I(\psi)$  represents the moment of inertia as a function of the hollow ratio. This equation gives the critical load for buckling, which applies to slender columns where the failure is dominated by instability rather than material strength.

#### Stress Concentrations around the Hollow Section

In HGBS columns, the edges around the hollow section experience increased stress concentration, especially near the corners or around the perimeter of the hollow core. These stress concentrations can lead to localized material failure, such as crack propagation or delamination, especially in composite materials like HGBS. To account for this, the local buckling load  $P_{local}$  needs to be considered, which is typically lower than the global buckling load. The local stress distribution depends on the shape of the hollow section and the material properties.

To analyze stress concentrations around the hollow section of HGBS columns, an analytical approach can be adopted that employs stress concentration factors (SCFs) and established engineering formulas to derive relevant stress values. The first step involves defining the geometric parameters of the hollow section, specifically the outer dimensions  $b_o$  (width) and  $h_o$  (height), along with the inner dimensions  $b_i$  (width) and  $h_i$  (height). The plate thicknesses can be expressed in Eqs. 5 and 6.

$$t_w = \frac{b_0 - b_i}{2t} \tag{5}$$

$$t_h = \frac{h_0 - h_i}{2t} \tag{6}$$

This moment of inertia quantifies the distribution of the cross-sectional area about the neutral axis, influencing the column's stability.

To account for the geometric discontinuity of the hollow section, the stress concentration factor  $K_t$  can be derived from empirical formulas specific to rectangular hollow sections (Pilkey *et al.* 2008). While various methods exist, a common approach approximates the SCF in Eq. 7.

$$K_t = 1 + 2(\frac{t_w}{b_o} + \frac{t_h}{h_o}) \tag{7}$$

This equation captures the geometric effects on stress distribution in the hollow section. Using the previously determined stress concentration factor, the maximum stress  $\sigma_{max}$  at the edges of the hollow section can be expressed in Eq . 8.

$$\sigma_{max} = K_t \sigma \tag{8}$$

This value indicates the peak stress concentration occurring at the edges of the

hollow section, providing insight into potential failure points. The matrix formulation provides a comprehensive way to relate stress components to strain components, capturing anisotropic behavior typical of composite materials like HGBS. This is particularly relevant in assessing how different directions of loading affect the overall behavior of the column. Use the calculated strains to assess whether the material is in the elastic or inelastic range. If inelastic, apply the tangent modulus  $E_t$  for further calculations, shown in Eq. 9.

$$\begin{bmatrix} \sigma_{x} \\ \sigma_{y} \\ \tau_{xy} \end{bmatrix} = \begin{bmatrix} E_{11} & E_{12} & 0 \\ E_{21} & E_{22} & 0 \\ 0 & 0 & G_{xy} \end{bmatrix} \begin{bmatrix} \epsilon_{x} \\ \epsilon_{y} \\ \gamma_{xy} \end{bmatrix}$$
(9)

 $E_{11}$  and  $E_{12}$  are the elastic modulus in the principal directions, while  $G_{xy}$  represents the shear modulus. This allows for the calculation of stresses based on corresponding strains under various loading conditions.

# Tangent Modulus Theory

For columns exhibiting inelastic behavior, such as intermediate or short HGBS columns, Euler's buckling theory is insufficient. The tangent modulus theory is more appropriate because it takes into account the non-linear stress-strain behavior of the material. As the material moves beyond the elastic range, its stiffness decreases, which is captured by the tangent modulus  $E_{\rm t}$ .

As the hollow ratio increases, the material available to resist both axial and bending stresses decreases, which directly affects the tangent modulus  $E_t$  used in the inelastic phase of loading. The reduction in material stiffens the structure less effectively as it undergoes plastic deformation, causing a more rapid decrease in the modulus of elasticity.

This relationship can be captured by introducing a hollow factor  $\eta$  to modify the tangent modulus in Eq. 10.

$$E_{t,hollow} = \eta E_t \tag{10}$$

The tangent modulus is the slope of the stress-strain curve in the plastic region and is often determined experimentally or through material models. The critical load in the inelastic region is calculated using a modified version of Euler's buckling equation, and it's shown in Eq. 11,

$$P_{t,hollow} = \frac{\pi^2 E_{t,hollow} I(\psi)}{(kl)^2} \tag{11}$$

where  $P_{t, hollow}$  represents the critical load accounting for inelastic behavior, and  $E_t$  is the tangent modulus, which is smaller than the elastic modulus due to the material's plastic deformation. k is the effective length factor, which depends on the boundary conditions.

# **Combined Approach for Intermediate Slenderness**

For columns with intermediate slenderness ratios, both buckling and material failure may occur. In such cases, the critical load is governed by whichever mechanism dominates, either buckling or inelastic deformation. Therefore, the overall critical load can be determined in Eq. 12.

$$P_{final} = min (P_{eff}, P_{cr,hollow}, P_{t,hollow})$$
(12)

where  $P_{\text{eff}}$  is the effective load calculated based on the material strength and cross-sectional area,  $P_{\text{cr,hollow}}$  is the critical buckling load calculated based on Euler's formula, and  $P_{\text{t,hollow}}$  is the critical buckling load calculated based on the Tangent Modulus Theory.

In this approach, the effective load capacity is the smaller of the Euler buckling load and the tangent modulus-based critical load. This ensures that both geometric instability and material nonlinearity are considered in determining the column's load-bearing capacity.

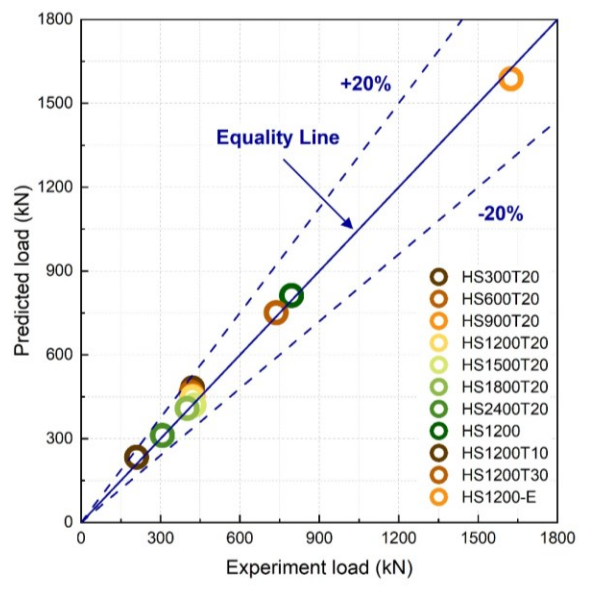


Fig. 10. Comparison between predicted load and experiment load

For slender HGBS columns, the Euler buckling load typically governs, and the material behaves elastically up to failure. In contrast, for short or squat columns, material strength is the limiting factor, and the tangent modulus theory provides a more accurate prediction. For intermediate columns, the combined approach ensures that both buckling and material plasticity are accounted for, giving a comprehensive prediction of the column's performance under axial load. Figure 10 presents a comparison between the predicted critical loads derived from the combined approach and experimental results. The predictions for all tested specimens were within a 20% margin of error, demonstrating the robustness and reliability of the proposed model. Notably, for columns with lengths exceeding 1200 mm, the error margin decreases to within 10%, highlighting the superior accuracy of this approach compared to conventional code-based predictions. The latter often rely on oversimplified assumptions and fail to account for the intricate interaction between buckling and material behavior. However, the model underestimates the critical load for the HS1200-E column, which features an enlarged cross-section of 180mm × 180 mm. This discrepancy may be attributed to size effects, such as reduced material efficiency or deviations in the stress distribution for larger sections. This observation indicates a potential limitation of the current model for columns with increased cross-sectional dimensions. Further studies are warranted to investigate and address the influence of size effects on predictive accuracy, particularly for large-section HGBS columns.

#### CONCLUSIONS

1. From the failure modes of hollow glued bamboo scrimber (HGBS) columns with equal slenderness and hollow ratio, it was found that the failure mode exhibited a certain degree of randomness. Most of the failure modes of were material failures, but some were in the failure mode of adhesive layer delamination. It is speculated that such

- failures arose due to the inhomogeneity of materials and adhesives due to events during the production process.
- 2. The slenderness ratio was found to have a certain influence on the bearing capacity and stability of HGBS columns. For short columns, it mainly manifested as strength failure. For medium and long columns, it mainly manifested as strength failure and instability failure. For long columns, it mainly manifested as instability failure. There was a critical slenderness ratio that affects the compressive bearing capacity of HGBS columns.
- 3. The hollow ratio is an important influencing factor for HGBS columns. Under the same material usage, HGBS columns can greatly improve their stiffness. However, it is not the case that the larger the hollow ratio, the higher the bearing capacity. It was found that there is a critical hollow ratio that can balance the material usage and load-bearing capacity.
- 4. For the calculation of the axial compression bearing capacity of HGBS column, calculation formulas were established, laying a theoretical groundwork for the application and promotion of HGBS columns in engineering.

#### **ACKNOWLEDGEMENTS**

This work was supported by Sichuan Science and Technology Program (2023YFS0393).

#### REFERENCES CITED

- ANSI/AF&PA (2005). *National Design Specification for Wood Construction*, American Forest and Paper Association, Washington DC, USA.
- Dauletbek, A., Li, H., and Lorenzo, R. (2023). "A review on mechanical behavior of laminated bamboo lumber connections," *Composite Structures* 313, article 116898. DOI: 10.1016/j.compstruct.2023.116898
- De Flander, K., and Rovers, R. (2009). "One laminated bamboo-frame house per hectare per year," *Construction and Building Materials* 23(1), 210-218. DOI: 10.1016/j.conbuildmat.2008.01.004
- Dewi, S. M., and Soehardjono, A. (2018). "The strength of axially loaded square hollow section column made of laminated Asian bamboo (*Dendrocalamus asper Becker*)," *Res. J. Appl. Sci. Eng. Technol.* 15(9), 337-343. DOI: 10.19026/rjaset.15.5924
- EN 1995 (2001). "Eurocode 5: Design of timber structures," European Committee for Standardization, Brussels, Belgium.
- Fei, B., Liu, R., Liu, X., Chen, X., and Zhang, S. (2019). "A review of structure and characterization methods of bamboo pits," *Journal of Forestry Engineering* 4(2) 4(2), 13-18.
- Feng, P., Qiang, H., and Ye, L. (2017). "Discussion and definition on yield points of materials, members and structures," *Engineering Mechanics* 34(3), 36-46. (in Chinese) DOI: 10.6052/j.issn.1000-4750.2016.03.0192
- GB 50005 (2003). "Wood structure design specification," Ministry of Housing and Urban-Rural Development of the People's Republic of China, Beijing. (in Chinese)

- GB/T 15777 (2017). "Method for determination of the modulus of elasticity in compression parallel to grain of wood," China National Standardization Administration, Beijing.
- GB/T 50329 (2012). "Standard test methods for timber structures," China National Standardization Administration, Beijing.
- Goonewardena, J., Ashraf, M., Subhani, M., Kafle, B., and Reiner, J. (2024). "Slenderness limits and buckling response of bamboo scrimber under axial compression," *Materials Science Forum* 1123, 53-58. DOI: 10.4028/p-naDnW6
- Jensen, J. L., and Quenneville, P. (2011). "Experimental investigations on row shear and splitting in bolted connections," *Construction and Building Materials* 25(5), 2420-2425. DOI: 10.1016/j.conbuildmat.2010.11.050
- Ke, Y. (2014). Experimental Research and Analysis of Structural Columns Made of Bamboo Scrimber for Framework Structures, Master's Thesis, Nanjing Forestry University. (in Chinese)
- Kumar, A., Vlach, T., Laiblova, L., Hrouda, M., Kasal, B., Tywoniak, J., and Hajek, P. (2016). "Engineered bamboo scrimber: Influence of density on the mechanical and water absorption properties," *Construction and Building Materials* 127, 815-827. DOI: 10.1016/j.conbuildmat.2016.10.069
- Kurt, R., and Tomak, E. D. (2019). "The effect of DMDHEU modification on physical and biological properties of parallel strand lumbers," *Construction and Building Materials* 195, 497-504. DOI: 10.1016/j.conbuildmat.2018.11.064
- Leng, Y., Wang, Z., and Xu, M. (2021). "Experimental study and analysis on rotational behavior of bamboo scrimber beam-to-column bolted connections," *J. Structural Engineering* 147(9), article 04021122. DOI: 10.1061/(ASCE)ST.1943-541X.0003099
- Li, H., Liu, R., Lorenzo, R., Wu, G., & Wang, L. B. (2019). "Eccentric compression properties of laminated bamboo columns with different slenderness ratios," *Proceedings of the Institution of Civil Engineers–Structures and Buildings* 172(5), 315-326. DOI: 10.1680/jstbu.18.00007
- Li, H., Su, J., Zhang, Q., Deeks, A. J., and Hui, D. (2015). "Mechanical performance of laminated bamboo column under axial compression," *Composites part B: Engineering* 79, 374-382. DOI: 10.1016/j.compositesb.2015.04.027
- Li, H., Zhang, Q., Huang, D., and Deeks, A. J. (2013). "Compressive performance of laminated bamboo," *Composites Part B: Engineering* 54, 319-328. DOI: 10.1016/j.compositesb.2013.05.035
- Li, H.-T., Su, J.-W., Zhang, Q.-S., Deeks, A. J., and Hui, D. (2015). "Mechanical performance of laminated bamboo column under axial compression," *Composites Part B: Engineering* 79, 374-382. DOI: 10.1016/j.compositesb.2015.04.027
- Li, Y., Xu, B., Zhang, Q., and Jiang, S. (2016). "Present situation and the countermeasure analysis of bamboo timber processing industry in China," *Journal of Forestry Engineering* 2016(1), 2-7.
- LY/T 3194 (2020). "Structural bamboo scrimber," State Forestry and Grassland Administration. (in Chinese)
- Mahdavi, M., Clouston, P., and Arwade, S. (2011). "Development of laminated bamboo lumber: Review of processing, performance, and economical considerations," *J. Mater. Civil Eng.* 23(7), 1036-1042. DOI: 10.1061/(ASCE)MT.1943-5533.0000253
- Meng, X., Zhang, Z., Wu, Y., Xu, F., and Feng, P. (2023). "A comprehensive evaluation of the effects of bamboo nodes on the mechanical properties of bamboo culms," *Engineering Structures* 297, article 116975. DOI: 10.1016/j.engstruct.2023.116975
- Pilkey, W. D., and Pilkey, D. F. (2008). Peterson's Stress Concentration Factors, 3rd Ed.,

- John Wiley & Sons, Hoboken, NJ, USA.
- Qi, J., Xie, J., Yu, W., and Chen, S. (2015). "Effects of characteristic inhomogeneity of bamboo culm nodes on mechanical properties of bamboo fiber reinforced composite," *Journal of Forestry Research* 26, 1057-1060.
- Sharma, B., and van der Vegte, A. (2020). "Engineered bamboo for structural applications," in: *Nonconventional and Vernacular Construction Materials*, Woodhead Publishing, Sawston, UK, pp. 597-623. DOI: 10.1016/B978-0-08-102704-2.00021-4
- Su, J., Wu, F., Li, H. and Yang, P. (2015). "Experimental study on axial compression of bamboo scrimber column," *Chinese J. Science and Technology* 10(01), 39-41+50. (in Chinese).
- Su, Y., and Zou, J. (2024). "Local stability of glued laminated bamboo columns with box sections under axial compression," *Eur. J. Wood Wood Prod.*, 1-15.
- Tan, C., Li, H., Ashraf, M., Corbi, I., Corbi, O., and Lorenzo, R. (2021). "Evaluation of axial capacity of engineered bamboo columns," *Journal of Building Engineering* 34, article 102039. DOI: 10.1016/j.jobe.2020.102039
- Wang, R., Xiao, Y., and Li, Z. (2017). "Lateral loading performance of lightweight glubam shear walls," *Journal of Structural Engineering* 143(6), article 04017020. DOI: 10.1061/(ASCE)ST.1943-541X.0001751
- Wang, X. (2020). Research on the Compression Performance and Ultimate Bearing Capacity of Bamboo and Wooden Components, Ph.D. Dissertation, Nanjing Forestry University. (in Chinese)
- Wei, H., Shi, D., Rupert, E., Fragiacomo, M., Demartino, C., and Xiao, Y. (2025). "Axial compressive behavior of novel laminated bamboo tubes: Experimental tests and predictive buckling model," *Construction and Building Materials* 463, article 139987. DOI: 10.1016/j.conbuildmat.2025.139987
- Wei, Y., Ji, X., Duan, M., and Li, G. (2017). "Flexural performance of bamboo scrimber beams strengthened with fiber-reinforced polymer," *Construction and Building Materials* 142, 66-82. DOI: 10.1016/j.conbuildmat.2017.03.054
- Xiao, Y., Li, Z., and Wang, R. (2015). "Lateral loading behaviors of lightweight wood-frame shear walls with ply-bamboo sheathing panels," *Journal of Structural Engineering* 141(3), article B4014004. DOI: 10.1061/(ASCE)ST.1943-541X.0001033
- Yang, Z., Hu, Y., and Qiu, X. (2020). "Study on bending properties of recombinant bamboo and glued bamboo," *IOP Conference Series: Materials Science and Engineering* 768(3). DOI: 10.1088/1757-899X/768/3/032029
- Zhang, M., Fan, H., Li, W., Wu, H., Yu, Z., Zhao, S., Zhao, Q., Chen, S., Behnejad, A., and Parke, G. (2024). "Experimental investigation on the dowel-bearing properties of *Neosinocalamus affinis*-based bamboo scrimber," *Engineering Structures* 304, article 117618. DOI: 10.1016/j.engstruct.2024.117618
- Zhong, Y., Wu, G., Ren, H., and Jiang, Z. (2017). "Bending properties evaluation of newly designed reinforced bamboo scrimber composite beams," *Construction and Building Materials* 143, 61-70. DOI: 10.1016/j.conbuildmat.2017.03.052
- Zhou, L., Shi, L., Xiong, G., Kang, S., Qin, Y., and Yan, H. (2023). "Global buckling behaviour of bamboo scrimber box columns under axial compression: Experimental tests and numerical modelling," *J. Build. Eng.* 63, article 105435. DOI: 10.1016/j.jobe.2022.105435

Article submitted: July 14, 2025; Peer review completed: August 9, 2025; Revised version received: August 29, 2025; Accepted: September 6, 2025; Published: September 16, 2025. DOI: 10.15376/biores.20.4.9678-9698